Raman and Theoretical Study of the Solvent Effects on the Sizable Intramolecular Charge Transfer in the Push−Pull 5-(Dimethylamino)-5′-nitro-2,2′-bithiophene

Enrique Ortí,*,[†] Pedro M. Viruela,[†] Rafael Viruela,[†] Franz Effenberger,[‡] Víctor Hernández,[§] and Juan T. López Navarrete*,[§]

Institut de Ciència Molecular, Universitat de València, E-46100 Burjassot (València), Spain, Institut für Organische Chemie der Universität Stuttgart, Pfaffenwaldring 55, D-70569 Stuttgart, Germany, and Departamento de Química Física, Universidad de Málaga, E-29071 Málaga, Spain

In this paper, we analyze the degree of intramolecular charge transfer in a push−pull π-conjugated system, 5-(dimethylamino)-5′-nitro-2,2′-bithiophene, from changes in frequencies and relative intensities of its strongest Raman scatterings in a bunch of solvents with different polarities. Density functional theory (DFT) was used as a support of the experimental study. Solvent effects on the molecular and electronic structures and on the vibrational properties were estimated by performing B3LYP/6-31G** calculations within the framework of the polarized continuum model (PCM) developed by Tomasi. Calculations reveal that the molecule is highly polarized in the ground state and behaves as a very efficient photoinduced push−pull system. The polarization of the molecule strongly increases with solvent polarity and determines that the profile of the Raman spectra greatly changes from one solvent to another and in going to the solid. The strongest Raman scattering associated with the $\nu_{sym}(NO_2)$ stretching undergoes a downshift of 48 cm^{-1} in passing from CCl$_4$ to the solid. DFT calculations provide a comprehensive interpretation of the evolution of the Raman spectra with solvent polarity.

I. Introduction

Dipolar push−pull chromophores are currently the subject of great interest for their use in photonic devices for telecommunications and optical information processing and represent the widest class of organic compounds investigated for their nonlinear optical (NLO) properties.[1−11] Push−pull NLO systems are basically constituted by an electron-donor and an electron-acceptor group interacting through a π-conjugated spacer. It is now well-established that the hyperpolarizability β, which characterizes the molecular NLO efficiency, depends on the strength of the donor/acceptor pair, on the extent of the π-conjugated path, and, for π-conjugated spacers made up of aromatic units, on the resonance stabilization energy of the aromatic systems.[4]

Oligoenic push−pull NLO-phores can be thought at first glance to constitute the most straightforward way to achieve an efficient charge redistribution from the donor to the acceptor end groups, and they have been demonstrated to exhibit huge nonlinearities.[5] However, these chromophores commonly lack the necessary chemical and photothermal stability, which limits their practical application in real devices. On the other hand, the large aromaticity of the benzene ring limits the efficiency of electron transmission in oligophenylene push−pull NLO-phores and has detrimental effects on the second-order polarizabilities. Since aromaticity of thiophene is lower than that of benzene and the stability and solubility of thiophene derivatives are higher than those of oligoenic compounds, much effort has been made over the past decade to the study of stable thiophene-based second-order NLO-phores.[5a,12]

One of us reported some years ago on the synthesis and the solvatochromic properties of a series of donor−acceptor end-capped oligothiophenes.[13] Among the large variety of push−pull bi-, ter-, and quaterthiophenes studied in that work, 5-(dimethylamino)-5′-nitro-2,2′-bithiophene (Me$_2$N-T$_2$-NO$_2$) was found to show a particularly pronounced positive solvatochromism.[13b] The UV−vis absorption maximum, λ_{max}, of Me$_2$N-T$_2$-NO$_2$ largely redshifts, as a function of the solvent polarity, from ∼466 nm in aliphatic solvents such as *n*-pentane or *n*-hexane to ∼577 nm in formamide. The dye was used as a suitable probe for the determination of solvent polarity[13b] and has been recently shown to be the dye with the greatest solvent sensitivity among a family of donor−acceptor substituted 2,2′-bithiophenes.[14] The effective electronic interaction between the ending groups is evident not only in the marked solvatochromism but also in the large values measured for the hyperpolarizability β.[15]

Since the beginning of the research in the field of conducting organic polymers, vis-near-IR electronic absorption and vibrational infrared and Raman spectroscopies have been successfully used in conjunction to investigate many different types of π-conjugated oligomers and polymers. Among these techniques, Raman spectroscopy has been shown to be particularly suited to (i) estimating the degree of π-conjugation in the pristine or neutral state,[16−18] (ii) characterizing the structure and extension of charge defects in doped materials,[19] and (iii) evaluating the efficiency of the intramolecular charge transfer in push−pull oligomers.[20,21] The effective conjugation coordinate (ECC) theory justifies the appearance of only a few, overwhelmingly strong Raman bands, on the basis of the existence of an effective electron−phonon coupling in the π-conjugated systems due to their quasi one-dimensional structures.[22] In aromatic and heteroaromatic polyconjugated systems, the so-termed *collective ECC vibrational coordinate* has the analytic form of a linear combination of ring C=C/C−C stretchings, which transform the aromatic structure of the ground electronic state to a quinoid

[†] Universitat de València.
[‡] Institut für Organische Chemie der Universität Stuttgart.
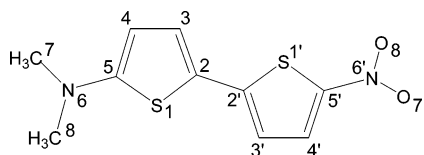[§] Universidad de Málaga.

Solvent Effects on Intramolecular Charge Transfer

J. Phys. Chem. A, Vol. 109, No. 39, 2005 **8725**

Figure 1. Chemical structure and atomic numbering of 5-(dimethylamino)-5-nitro-2,2′-bithiophene.

structure usually associated with electronically excited states or oxidized forms. The ECC formalism states that, as the length of the π-conjugated backbone increases, the totally symmetric normal modes involved in the molecular dynamics of the ECC coordinate (i.e., those giving rise to the intense Raman bands) undergo sizable dispersions both in peak positions and relative intensities. Frequency changes of Raman bands upon chain elongation are particularly useful in evaluating the *effective conjugation length* along a given series of neutral π-conjugated oligomers. On the other hand, when π-conjugated oligomers (particularly oligothiophenes) become chemically or electrochemically oxidized or photoexcited, typically, quinoid-like conjugational defects are created.[23] These structural changes also induce a sizable redshift of the Raman bands associated to the skeletal vibrations of the π-conjugated path.[16−19]

In this work, we focus on the Raman analysis of the intramolecular charge transfer in 5-(dimethylamino)-5′-nitro-2,2′-bithiophene (see Figure 1) as a function of the solvent polarity. The strongest Raman bands are found to downshift sizeably with increasing medium polarity. We also attempt to account for the solvent effects on geometrical, vibrational, and electronic properties of this push−pull system by performing density functional theory (DFT) calculations in the framework of the polarized continuum model (PCM) of Tomasi.[24] Calculations nicely reproduce the experimental trends.

II. Experimental and Theoretical Details

A. Raman Spectra. FT-Raman spectra were collected by using a Bruker FRA106/S accessory fitted to a Bruker Equinox 55 Fourier transform infrared absorption (FTIR) spectrometer. Data were collected in a typical backscattering configuration, and the operating power of the 1064 nm Nd:YAG laser radiation used as Raman excitation was kept to 500 mW in all experiments. The sample was analyzed as a pure solid in a sealed Raman capillary as well as in CCl_4, CH_2Cl_2, and DMSO solutions (solvents of analytical grade were purchased from Aldrich). Five thousand scans with 2 cm^{-1} spectral resolution were averaged to optimize the signal-to-noise ratio. Raman spectra of solutes were obtained, in all cases, after properly subtracting the Raman scatterings from the solvent. UV−vis absorption maxima of the three freshly prepared solutions were as follows: 489 nm (CCl_4), 535 nm (CH_2Cl_2), and 563 nm (DMSO) in accord with previously recorded data.[13b]

B. Computational Methods. DFT calculations were carried out as implemented in the *Gaussian 03* package of quantum chemical programs.[25] All calculations, which include geometry optimizations, electronic excitation energies, and vibrational spectra, were performed by using the Becke's three-parameter exchange functional in combination with the LYP correlation functional (B3LYP)[26] and the standard 6-31G** basis set.[27] Optimal geometries were determined on isolated entities and in three different solvents (CCl_4, CH_2Cl_2, and DMSO). On the resulting molecular geometries, harmonic vibrational frequencies and intensities were calculated analytically. DFT//B3LYP force fields have been shown to yield vibrational spectra in very good agreement with experiment[28,29] and have been widely and

successfully applied to study the vibrational properties of oligothiophenes.[16−19] The nowadays usual and handy adjustment of the theoretical force field, in which vibrational frequencies are uniformly scaled down by a factor of 0.96, was used throughout the work following the recommendations by Scott and Radom.[28] This scaling procedure even if quite simple is accurate enough to disentangle serious misassignments. Thus, all vibrational frequencies reported throughout the paper correspond to scaled values. DFT//B3LYP/6-31G** Raman spectral profiles of Me_2N-T_2-NO_2 in the various solvents studied were simulated by convoluting the scaled frequencies with Gaussian functions and assuming a constant bandwidth at the half-height of 10 cm^{-1}. The relative heights of the Gaussians were determined from the theoretical Raman scattering activities. Vertical electronic excitation energies were computed for the fifteen lowest-energy excited states by using the time-dependent DFT (TDDFT) approach[30−32] and the molecular geometries previously optimized.

Solvent effects on the Raman and electronic spectra were also considered by recalculating the harmonic force fields and the vertical excitation energies within the SCRF (self-consistent-reaction-field) theory using the PCM approach to model the interaction with the solvent.[33] The PCM model considers the solvent as a continuous medium with a dielectric constant, ϵ, and represents the solute by means of a cavity built with a number of interlaced spheres.[24] Raman scattering calculations in solution were performed using the equilibrium approach or the static description for the dielectric response of the solvent, i.e., without taken into account the fact that the solvent cannot instantaneously readjust to the oscillations in time of the solute charge density produced by solvent vibrations or by the polarization induced in the solute by the incident electromagnetic field. Raman intensities can be sensitive to this kind of nonequilibrium or dynamics effects.[34,35] Net atomic charges were calculated using the natural population analysis (NPA)[36] included in the natural bond orbital (NBO) algorithm proposed by Weinhold and co-workers.[37]

III. Results and Discussion

A. Molecular Structure and Electronic Properties. The molecular geometry of Me_2N-T_2-NO_2 was first optimized for the isolated molecule without imposing any symmetry restriction and assuming an anti arrangement of the thienyl rings. The optimized B3LYP/6-31G** structure is almost completely planar in agreement with previously published crystallographic X-ray data.[13a] The thienyl rings are slightly rotated around the central C2−C2′ bond (B3LYP/6-31G**, 4.0°; X-ray, 3.7°), and the amine nitrogen is theoretically predicted to be slightly pyramidalized. Table 1 collects the bond lengths calculated for Me_2N-T_2-NO_2 together with solid X-ray data.[13a] The values obtained at the B3LYP/6-31G** level for unsubstituted 2,2′-bithiophene (T_2), 5,5′-bis(dimethylamino)-2,2′-bithiophene (Me_2N-T_2-NMe_2), and 5,5′-dinitro-2,2′-bithiophene (NO_2-T_2-NO_2) are also included in Table 1 for comparison purposes.

Data in Table 1 indicate that the conjugated C=C/C−C chain of the bithiophene molecule is significantly affected by α,α′-substitution and that the effect of the electron-withdrawing nitro groups in NO_2-T_2-NO_2 is more pronounced than the effect of the electron-releasing dimethylamino groups in Me_2N-T_2-NMe_2. For Me_2N-T_2-NO_2, the degree of bond length alternation (BLA), calculated as the difference between the average lengths of the π-conjugated C−C and C=C bonds, amounts to 0.025 and 0.029 Å for the thienyl rings attached to the NO_2 and NMe_2 groups, respectively. These values are much smaller than those obtained

TABLE 1: B3LYP/6-31G**-Optimized Bond Lengths (in Å) for α,α′-Substituted 2,2′-Bithiophenes

bond	$Me_2N\text{-}T_2\text{-}NO_2{}^a$	$T_2{}^b$	$Me_2N\text{-}T_2\text{-}NMe_2{}^b$	$NO_2\text{-}T_2\text{-}NO_2{}^b$
C2−C2′	1.436 (1.438)	1.451	1.447	1.447
C2−C3	1.379 (1.372)	1.378	1.373	1.387
C2′−C3′	1.393 (1.385)	1.378	1.373	1.387
C3−C4	1.412 (1.402)	1.424	1.425	1.412
C3′−C4′	1.408 (1.399)	1.424	1.425	1.412
C4−C5	1.388 (1.383)	1.367	1.379	1.372
C4′−C5′	1.374 (1.363)	1.367	1.379	1.372
C5−N6	1.371 (1.356)		1.388	1.434
C5′−N6′	1.421 (1.417)		1.388	1.434
N6−C7	1.456 (1.445)		1.454	
N6−C8	1.456 (1.423)		1.458	
N6′−O7	1.237 (1.237)			1.232
N6′−O8	1.240 (1.240)			1.236

[a] Experimental solid-state X-ray values from ref 13a are given within parentheses. [b] Geometries optimized within C_2 symmetry constraints.
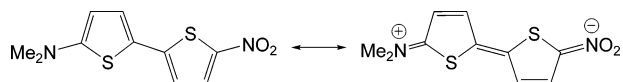
Figure 2. Neutral and charge-separated limiting resonance forms for $Me_2N\text{-}T_2\text{-}NO_2$.

for T_2 (0.051 Å) and $Me_2N\text{-}T_2\text{-}NMe_2$ (0.049 Å) and are even lower than that obtained for $NO_2\text{-}T_2\text{-}NO_2$ (0.032 Å). Therefore, the presence of the acceptor group in $Me_2N\text{-}T_2\text{-}NO_2$ strongly polarizes the π-electron cloud of the conjugated spacer and equalizes the lengths of the CC bonds in both thienyl rings. The polarization effect is in fact much larger than that obtained for the closely related $Me_2N\text{-}T_2\text{-}CN$ push−pull system. In $Me_2N\text{-}T_2\text{-}CN$, both the thienyl ring linked to the electron-acceptor CN group and the thienyl ring attached to the electron-donor NMe_2 group show higher BLA values (0.030 and 0.035 Å, respectively). The greater electron polarization occurring in $Me_2N\text{-}T_2\text{-}NO_2$ is also suggested by the shorter length calculated for the central C2−C2′ bond (1.436 Å) in comparison with that obtained for $Me_2N\text{-}T_2\text{-}CN$ (1.440 Å). Structural data therefore indicate that a more effective intramolecular charge transfer takes place in $Me_2N\text{-}T_2\text{-}NO_2$.

The molecular structure of $Me_2N\text{-}T_2\text{-}NO_2$ can be thus viewed as a mixing of the two limiting resonant forms sketched in Figure 2. In the neutral form, no intramolecular charge transfer takes place from the donor to the acceptor, and the central spacer displays a fully aromatic structure. In the charge-separated form, one electron is fully transferred from the donor to the acceptor, and the π-conjugated spacer becomes fully quinoidized. The relative stability of the zwitterionic form with respect to the neutral form determines the weight of the contributions of these two canonical structures to the linear combination that describes the structure of the push−pull chromophore.

To gain a deeper insight into the polarization of the push−pull $Me_2N\text{-}T_2\text{-}NO_2$ system, the net charges accumulated by the different structural moieties were calculated using the NPA algorithm. As summarized in Table 2, the negative charge supported by the acceptor group (−0.33 e) is much higher than the positive charge located over the donor NMe_2 group (+0.01 e), which remains almost neutral. The charge of the NO_2 group is balanced by the bithienyl spacer, which bears positive charges of +0.20 and +0.12 e on the thienyl rings linked to the acceptor and donor groups, respectively.[38] The inductive effect of the NO_2 group thus polarizes the whole π-conjugated backbone and drastically reduces the aromatic character of both thienyl rings. It is to be noted that the charge distribution obtained for $Me_2N\text{-}T_2\text{-}NO_2$ is markedly different from that calculated for $Me_2N\text{-}T_2\text{-}CN$. In this molecule, both the CN and NMe_2 groups show

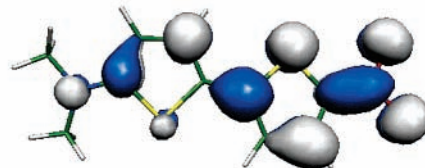**TABLE 2: B3LYP/6-31G**-NPA Charges (in e) Calculated in Different Media for the Chemical Groups Constituting the $Me_2N\text{-}T_2\text{-}NO_2$ Molecule**

solvent	NMe_2	$T(NMe_2){}^a$	$T(NO_2){}^a$	NO_2
isolated molecule	+0.01	+0.12	+0.20	−0.33
CCl_4	+0.04	+0.13	+0.20	−0.37
CH_2Cl_2	+0.06	+0.15	+0.21	−0.43
DMSO	+0.08	+0.16	+0.21	−0.45

[a] $T(NMe_2)$ and $T(NO_2)$ denote the thienyl rings attached to the NMe_2 and NO_2 groups, respectively.
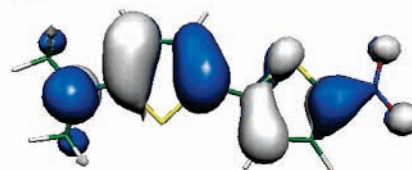
Figure 3. Electron density contours calculated for the HOMO and the LUMO of $Me_2N\text{-}T_2\text{-}NO_2$.

small charges (−0.05 and 0.00 e, respectively), and their adjacent thienyl rings have charges of opposite sign (−0.05 and +0.10 e, respectively).

The optical properties of $Me_2N\text{-}T_2\text{-}NO_2$ were also investigated by calculating the lowest-energy electronic excited states using the TDDFT approach. Experimentally, the UV−vis spectrum of $Me_2N\text{-}T_2\text{-}NO_2$ presents an intense band (ϵ_{max} = 25 000 L mol^{-1} cm^{-1}) with maximum absorption at 466.2 nm (2.66 eV) in apolar solvents such as *n*-hexane.[13] Time-dependent (TD)-DFT calculations predict the occurrence of only one electronic transition in the visible region at 2.78 eV with an oscillator strength (*f*) of 0.61 (the next active transition appears at 4.03 eV (*f* = 0.18)). The transition corresponds to a π → π* excitation to the first excited electronic state and is mainly described by a one-electron promotion from the highest occupied molecular orbital (HOMO) to the lowest unoccupied molecular orbital (LUMO). Although both orbitals spread over the whole molecule, the HOMO presents a larger electron density around the donor group, and the LUMO mostly lies on the acceptor part of the molecule (see Figure 3). The absorption band observed experimentally therefore arises from a single electronic transition, in agreement with electrooptic absorption measurements,[13a,15] and implies an electron density transfer from the electron-donating to the electron-accepting moiety.

The charge-transfer nature of the optical absorption band is supported by the enhancement of the dipole moment associated to the electronic transition. Experimentally, it is measured to increase by a factor of 2.75 in passing from the ground state (8 D, in benzene) to the excited state (22 D).[13a,15] Theoretically, it is calculated to augment by a similar factor, from 10.5 to 26.0 D, for the isolated molecule. In comparison, the dipole moment of the $Me_2N\text{-}T_2\text{-}CN$ system, which presents an absorption maximum at 398 nm (3.12 eV)[13b] calculated at 3.20 eV (*f* = 0.69), is computed to increase from 9.2 to 19.7 D with the electronic transition. Calculations therefore suggest that Me_2N-

Solvent Effects on Intramolecular Charge Transfer

J. Phys. Chem. A, Vol. 109, No. 39, 2005 **8727**

TABLE 3: B3LYP/6-31G** Optimized Bond Lengths (in Å) Calculated for Me$_2$N-T$_2$-NO$_2$ in Different Solvents

bond	isolated molecule	CCl$_4$	CH$_2$Cl$_2$	DMSO
C2−C2′	1.436	1.430	1.426	1.423
C2−C3	1.379	1.382	1.385	1.386
C2′−C3′	1.393	1.395	1.399	1.400
C3−C4	1.412	1.408	1.404	1.403
C3′−C4′	1.408	1.405	1.401	1.400
C4−C5	1.388	1.391	1.395	1.396
C4′−C5′	1.374	1.376	1.379	1.380
C5−N6	1.371	1.364	1.359	1.356
C5′−N6′	1.421	1.413	1.405	1.401
N6−C7	1.456	1.456	1.459	1.459
N6−C8	1.456	1.456	1.456	1.456
N6′−O7	1.237	1.239	1.242	1.244
N6′−O8	1.240	1.243	1.246	1.248

T$_2$-NO$_2$ behaves as a more efficient push−pull system than Me$_2$N-T$_2$-CN both in the ground state and as a photoinduced charge-transfer compound.

B. Solvent Effects. To evaluate the influence of the solvent, the structural and electronic properties of Me$_2$N-T$_2$-NO$_2$ were recalculated in CCl$_4$, CH$_2$Cl$_2$, and DMSO using the PCM approach. As expected, the molecule becomes more polarized in the presence of the solvent (see Table 2), and the molecular dipole moment increases with solvent polarity (CCl$_4$, 12.5 D; CH$_2$Cl$_2$, 14.7 D; DMSO, 15.4 D).

Table 3 summarizes the values of selected bond lengths calculated in the different solvents. The largest changes correspond to the C$_\alpha$−N bonds connecting the donor and acceptor groups to the bithienyl spacer that undergo shortenings of 0.015 and 0.020 Å, respectively, in passing from the isolated molecule to DMSO. These changes are accompanied by a shortening of the central C$_\alpha$−C$_{\alpha'}$ bond (0.013 Å) and by a reduction of the BLA values calculated for the respective thienyl rings, which decrease from 0.029 and 0.025 Å in the isolated molecule to 0.011 and 0.010 Å in DMSO. Thus, the quinoidization induced by the intramolecular charge transfer taking place in Me$_2$N-T$_2$-NO$_2$ significantly increases in going to more polar media. In other words, the charge-separated quinoid form sketched in Figure 2 contributes more to the structure of the push−pull chromophore.

Calculations show that the interaction with the solvent has a different effect on the frontier orbitals of Me$_2$N-T$_2$-NO$_2$. While the energy of the HOMO slightly increases with solvent polarity, that of the LUMO decreases, and the HOMO−LUMO energy gap becomes narrower. This monoelectronic picture can be used as a first-approach explanation of the positive solvatochromism exhibited by Me$_2$N-T$_2$-NO$_2$. The absorption maximum shifts from 466.0 nm (2.66 eV) in a nonpolar solvent like *n*-hexane to 563.2 nm (2.20 eV) in a polar solvent like DMSO.[13b] As discussed above, the absorption is due to a charge-transfer electronic transition that implies a huge increase of the molecular dipole moment. The interaction of polar solvents with the solute molecules therefore produces a higher stabilization of the excited state, and the energy of the transition decreases with solvent polarity. TDDFT-PCM calculations provide excitation energies of 2.57 eV ($f = 0.75$) in *n*-hexane, 2.54 eV ($f = 0.77$) in CCl$_4$, 2.46 eV ($f = 0.82$) in CH$_2$Cl$_2$, and 2.42 eV ($f = 0.85$) in DMSO.[39] Thus, the calculations correctly predict the bathochromic shift and the increase of intensity with solvent polarity, but they underestimate the magnitude of the shift.

C. Raman Spectra. Figure 4 displays the FT-Raman spectra of Me$_2$N-T$_2$-NO$_2$ as a solute in CCl$_4$, CH$_2$Cl$_2$, and DMSO solutions as well as a pure solid sample. Table 4 correlates the wavenumbers measured for the main Raman scatterings in the
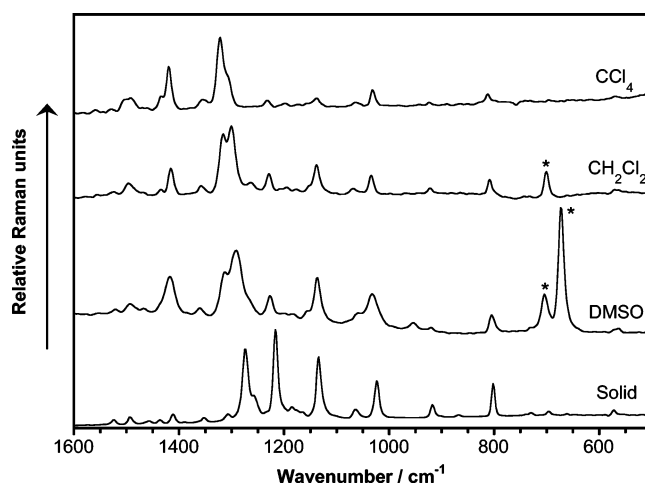

Figure 4. FT-Raman spectra of Me$_2$N-T$_2$-NO$_2$ recorded in CCl$_4$, CH$_2$-Cl$_2$, and DMSO solutions and in solid state over probe energies of 1600−500 cm^{-1}. Arterisks denote solvent bands.

TABLE 4: Vibrational Raman Frequencies (in cm^{-1}) Measured for Me$_2$N-T$_2$-NO$_2$ in Different Solvents and in Solid State

CCl$_4$	CH$_2$Cl$_2$	DMSO	solid
1419	1417	1414	1411
1322	1317	1312	1306
1306	1301	1290	1274
1232	1230	1226	1216
1137	1137	1136	1134
1032	1033	1036	1023
813	808	804	802

different media. We first observe that the sample exhibits the spectroscopic characteristics commonly found for many classes of π-conjugated molecular materials: (i) The Raman spectrum shows an unexpectedly simple appearance for a system, like Me$_2$N-T$_2$-NO$_2$, which has a complex structure and lacks any molecular symmetry element (i.e., mirror planes, *n*-fold rotation axis of symmetry, center of symmetry, and so on),[16−18,22] and (ii) Raman lines associated to particular stretching vibrations are found to display intensities much stronger than most of the Raman-active normal modes.[18e] We also observe that, similarly to other highly polarized oligothiophenes end-capped with electron-donor and electron-acceptor groups,[20,21] Me$_2$N-T$_2$-NO$_2$ displays an increased number of Raman scatterings as compared with nonpolar unsubstituted oligothiophenes[16,17] or with oligothienyl chains symmetrically end-capped with non-electroactive groups.[18]

The Raman spectra of nonpolar oligothiophenes usually show only four characteristic lines, overwhelmingly enhanced with respect to the other Raman-active vibrations predicted by the optical selection rules.[18] As mentioned in the Introduction, the observation of this phenomenon for pristine π-conjugated polymers was rationalized, in terms of lattice dynamics, by assuming the existence of a large electron−phonon coupling in these quasi one-dimensional systems.[22] As for the nonpolar oligothiophenes, the few Raman lines were termed as lines A, B, C, and D and were assigned to the following vibrations:

(i) Line A is due to a ν_{asym}(C=C) stretching, along which the two C=C bonds of each thienyl ring vibrate out-of-phase (i.e., asymmetrically) and the displacements of symmetry-equivalent atoms from their equilibrium positions occur fully in-phase (i.e., the corresponding normal vibration belongs to the totally symmetric species).[18a,22]

(ii) Line B is always the strongest Raman scattering and is associated to a totally symmetric ν_{sym}(C=C) stretching having
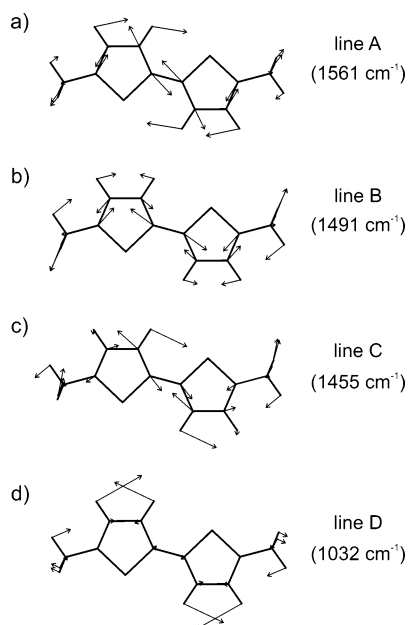
Figure 5. Schematic eigenvectors calculated at the B3LYP/6-31G** level for the most intense Raman-active symmetric vibrations of Me-T_2-Me (C_2 symmetry). Calculated wavenumbers are given within parentheses.

a *collective character,* since it spreads over the whole π-conjugated backbone, and along it, all thiophene rings vibrate in-phase and with similar amplitudes.

(iii) Line C is usually recorded with some intensity only for α- and β-substituted oligothiophenes,[18,19,22] while it is rather weak for unsubstituted oligothiophenes.[16,17] Its associated vibrational eigenvector is similar to that of line B, having also a marked collective character, with the difference that now the motions of the adjacent rings take place out-of-phase.

(iv) Finally, line D arises from a totally symmetric δ_{sym}(C$-$H) in-plane bending of the hydrogens attached to the β-positions of the thiophene rings and is mechanically coupled to line B.

To illustrate the vibrational nature of lines A, B, C, and D, Figure 5 sketches the eigenvectors (atomic vibrational displacements) calculated for the normal modes associated to these lines for α,α'-dimethylbithiophene (Me-T_2-Me). At the B3LYP/6-31G** level, the vibrational modes giving rise to lines A, B, and D are respectively computed at 1561, 1491, and 1032 cm^{-1}, in good agreement with the wavenumbers observed experimentally for solid Me-T_2-Me (1560, 1492, and 1045 cm^{-1}).[18a,40] The normal vibration associated to line C is calculated at 1455 cm^{-1}, but it has almost no intensity for Me-T_2-Me.

Upon oxidative doping to form radical cations and dications, the structure of oligothiophenes becomes more quinoid-like. This structural change is evidenced in the Raman spectra by a large displacement toward lower frequencies of the strongest line B, which shifts from $\sim$1480 cm^{-1} for neutral oligothiophenes, to $\sim$1440 cm^{-1} for radical cations, and to $\sim$1415 cm^{-1} for dications.[19] The shift has been attributed to the large softening of the conjugated double bonds induced by quinoidization.

The situation for the class of highly polarized push$-$pull oligothiophenes such as Me$_2$N-T_2-NO$_2$ is markedly different. On one hand, Me$_2$N-T_2-NO$_2$ presents a molecular structure intermediate between the aromatic structure of neutral α,α'-oligothiophenes and the quinoid structure of the cations/dications. On the other hand, two different molecular domains coexist in the bithienyl backbone of Me$_2$N-T_2-NO$_2$; the thienyl ring attached to the donor group displays a structure slightly more aromatic than the thienyl ring attached to the acceptor
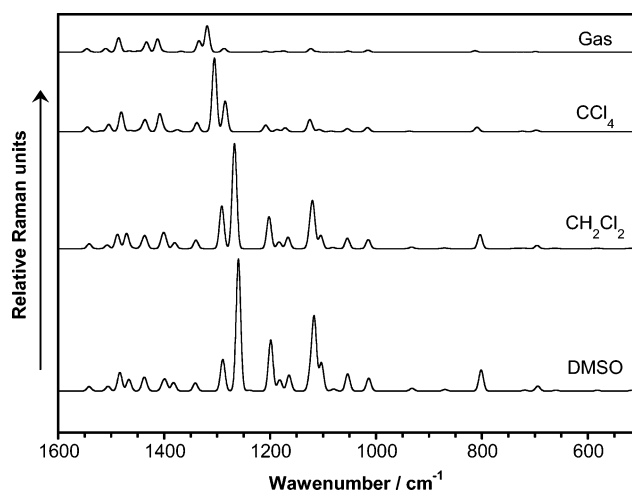

Figure 6. B3LYP/6-31G** Raman spectra calculated for Me$_2$N-T_2-NO$_2$ in gas phase and in CCl$_4$, CH$_2$Cl$_2$, and DMSO solutions.

group. The recognition of the characteristic Raman lines A, B, C, and D is therefore not straightforward in this class of compounds, and they are commonly found to split into two components associated to the two structural environments that coexist in the molecule. Thus, for this class of push$-$pull materials, it is especially useful to compute the Raman spectrum before reaching any empirical conclusion.

We have previously found for some push$-$pull systems incorporating a bithienylene-like spacer that their Raman profiles, in the form of a solute in a bunch of solvents, were almost superposable to those of the corresponding solids, independent of the solvent polarity.[21b,d] For Me$_2$N-T_2-NO$_2$, we find a different behavior. As observed in Figure 4, the Raman profile greatly changes from one solvent to another and in going to the solid. The strongest Raman features undergo a continuous redshift in passing from CCl$_4$ (1419, 1322, 1306 cm^{-1}), to CH$_2$-Cl$_2$ (1417, 1317, 1301 cm^{-1}), to DMSO (1414, 1313, 1290 cm^{-1}), and to the pure solid (1411, 1306, 1274 cm^{-1}). This shift is accompanied by important changes in the relative intensity of the bands. While the bands above 1400 cm^{-1} decrease in intensity, those below 1300 cm^{-1} augment their relative intensity with solvent polarity, and additional growing features are observed at 1225, 1135, 1030, and 810 cm^{-1}. To account for these observations, the influence of the solvent on the Raman vibrational properties is theoretically analyzed in the next section.

D. Theoretical Raman Spectra. Figure 6 illustrates the evolution of the Raman spectrum, calculated for Me$_2$N-T_2-NO$_2$ at the B3LYP/6-31G** level using the PCM model, upon changing the dielectric constant of the solvent. The "gas-phase" spectrum, evaluated on an isolated molecule, is also displayed for comparison purposes. Figure 7 correlates the experimental spectrum recorded in CCl$_4$ solution with the respective B3LYP/6-31G** spectrum. The theoretical spectra nicely reproduce the peak positions and relative intensities of the Raman lines (see Figure 7) and correctly predict the evolution of the Raman profile with the solvent polarity (cf. Figures 4 and 6).

The experimental Raman spectra show two main bands in the 1600$-$1400 cm^{-1} region (see Figures 4 and 7). The first band has a medium intensity and presents a double-peak structure (1504 and 1491 cm^{-1}) in CCl$_4$ solution. Calculations assign this band to the two vibrations computed at 1505 and 1481 cm^{-1}, which are associated to ν_{asym}(C=C) motions of the thienyl rings coupled with the asymmetric stretching of the NO$_2$ group. The contribution of this group increases with the polarity
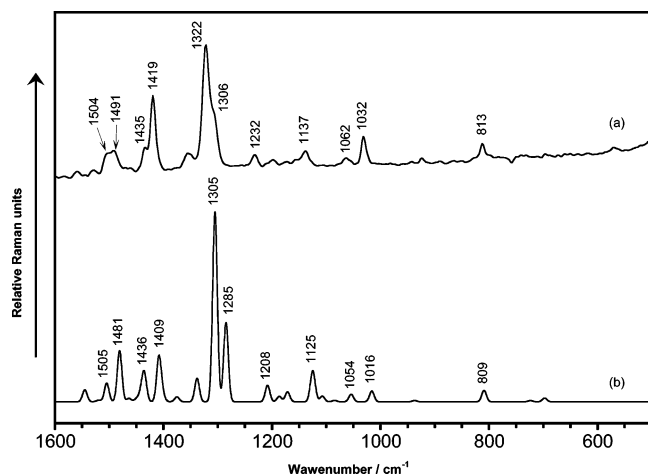
Solvent Effects on Intramolecular Charge Transfer

J. Phys. Chem. A, Vol. 109, No. 39, 2005 **8729**

Figure 7. Comparison of the experimentally recorded (a) and theoretically calculated (B3LYP/6-31G**) (b) Raman spectra of Me$_2$N-T$_2$-NO$_2$ in CCl$_4$ solution over probe energies of 1600−500 cm^{-1}.
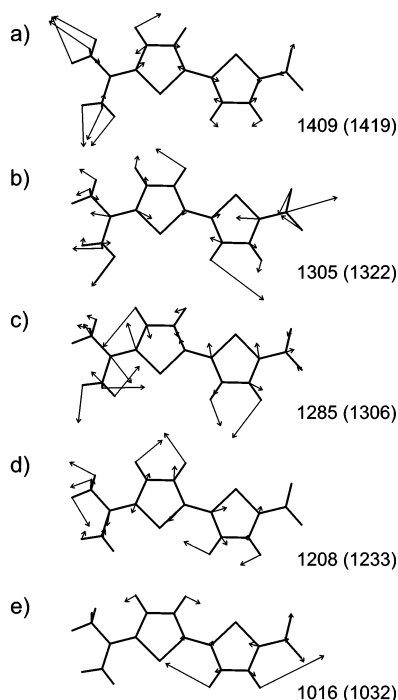

Figure 8. B3LYP/6-31G** eigenvectors calculated for selected normal modes of Me$_2$N-T$_2$-NO$_2$ in CCl$_4$ solution. Calculated and experimental (within parentheses) wavenumbers are given in cm^{-1}.

of the solvent, and both vibrations shift to lower frequencies and reverse their relative intensities (see Figure 6). In DMSO, they are calculated at 1485 and 1467 cm^{-1}, in good accord with the observed values (1493 and 1466 cm^{-1}). The vibrational mode corresponding to line A of α,α′-dimethylbithiophene (Figure 5a) is calculated at about 1545 cm^{-1} and is observed as a very weak band at ∼1560 cm^{-1}.

The band recorded at 1419 cm^{-1} (CCl$_4$ solution) undergoes a slight shift in passing to DMSO (1414 cm^{-1}) and presents a shoulder at about 1435 cm^{-1}. Calculations attribute this band to the peaks at 1436 and 1409 cm^{-1} (see Figure 7), which are due to δ(C−H) motions of the CH$_3$ groups with some contribution of the C−C stretchings of the spacer. In particular, the peak at 1409 cm^{-1} results from the vibrational normal mode depicted in Figure 8a and mainly involves the umbrella motion of the CH$_3$ groups. The mode includes some ν$_{sym}$(C=C) stretching of the thienyl rings that recalls the mode associated to line B

calculated at 1491 cm^{-1} for Me-T$_2$-Me (see Figure 5b). The mode appears at much lower frequencies for Me$_2$N-T$_2$-NO$_2$, owing to the softening of the π-conjugated backbone induced by the intramolecular charge transfer that equalizes the C=C/C−C bonds. The peak theoretically downshifts from 1409 cm^{-1} (in CCl$_4$) to 1402 cm^{-1} (in DMSO) in agreement with the experiment.

The strongest Raman scattering in CCl$_4$ solution appears at 1322 cm^{-1} with a shoulder at ∼1306 cm^{-1}. As the polarity of the solvent increases, the low-frequency feature gains in intensity, and both scatterings shift to lower frequencies (CH$_2$-Cl$_2$, 1317 and 1301 cm^{-1}; DMSO, 1312 and 1290 cm^{-1}) (see Figure 4). Calculations predict that the scatterings are mainly due to vibrations of the donor and acceptor groups, although coupled with motions of the π-conjugated spacer. In CCl$_4$ solution, the experimental line at 1322 cm^{-1} is due to the normal vibration calculated at 1305 cm^{-1} (see Figure 7). This vibration is mainly associated to a mixture of the symmetric ν$_{sym}$(NO$_2$) stretching of the acceptor group with the in-phase stretching of the two end C$_α$−N bonds (see Figure 8b). The shoulder at 1306 cm^{-1} is assigned to the less intense vibration calculated at 1285 cm^{-1}, which implies the ν$_{asym}$(N−C$_{Me}$) stretching of the donor group mixed with a ring ν(C=C) stretching (see Figure 8c). In passing to CH$_2$Cl$_2$ and DMSO, the two vibrations are calculated to interchange their positions. While the ν$_{sym}$(NO$_2$) vibration moves to lower frequencies (CH$_2$Cl$_2$, 1268 cm^{-1}; DMSO, 1260 cm^{-1}) and increases its intensity, the vibration associated with the ν$_{asym}$(N−C$_{Me}$) stretching slightly shifts to higher frequencies (CH$_2$Cl$_2$, 1292 cm^{-1}; DMSO, 1290 cm^{-1}). This crossing fully explains the evolution of the experimental band (see Figure 4). As the polarity of the solvent increases, the most intense peak associated to the ν$_{sym}$(NO$_2$) stretching downshifts from 1322 to 1290 cm^{-1}, gains in intensity, and interchanges its position with the less intense feature attributed to the ν$_{asym}$(N−C$_{Me}$) motion that slightly upshifts from 1306 to 1312 cm^{-1}.

The experimental Raman spectra present three bands in the 1250−1000 cm^{-1} region that increase in intensity with solvent polarity (see Figure 4). The first band appears at 1232 cm^{-1} and slightly shifts to lower frequencies in going to CH$_2$Cl$_2$ (1230 cm^{-1}) and DMSO (1226 cm^{-1}). The second and third bands are found at 1137 and 1032 cm^{-1}, respectively, and their positions remain mainly unaffected upon changing the solvent. B3LYP/6-31G** calculations nicely reproduce these trends (cf. Figures 4, 6, and 7). The first band is calculated at 1208 cm^{-1} in CCl$_4$ and downshifts in passing to CH$_2$Cl$_2$ (1202 cm^{-1}) and DMSO (1199 cm^{-1}). It is due to the vibrational mode sketched in Figure 8d that mainly implies the donor environment. The second band results from the mixing of two vibrational motions respectively associated to the acceptor and donor groups and is calculated at 1125 cm^{-1}. The third band arises from the δ$_{sym}$-(C−H) in-plane bending of the hydrogens attached to the β-positions of the thienyl rings and clearly corresponds to line D of α,α′-dimethyloligothiophenes (cf. Figure 5d and 8e). For Me$_2$-T$_2$-NO$_2$, the line actually splits into two components, calculated at 1054 and 1016 cm^{-1}, that are associated to the donor and acceptor environments, respectively. The two components are clearly observed in the Raman spectra recorded in CCl$_4$ (1062 and 1032 cm^{-1}) and CH$_2$Cl$_2$ (1068 and 1034 cm^{-1}) solutions (see Figure 4).

The increase in intensity with solvent polarity of the Raman bands below 1300 cm^{-1} can be related with the polarization of the C−H and N−O bonds involved in the vibrations associated to these bands. As the polarity of the solvent increases, these bonds become more polarized, the charges supported by

8730 *J. Phys. Chem. A, Vol. 109, No. 39, 2005*

Ortí et al.

hydrogen and oxygen atoms are higher, and larger changes of the molecular polarizability should be therefore expected during the molecular vibrations. Since the intensities of the Raman bands depend on the magnitude of these changes, higher Raman intensities are found for more polar solvents.

Finally, an experimental band is observed at ∼800 cm⁻¹ that grows in intensity and shifts down in frequency with solvent polarity (CCl₄, 813 cm⁻¹; CH₂Cl₂, 808 cm⁻¹; DMSO, 804 cm⁻¹). Calculations accurately predict the intensity increase and the frequency downshift (CCl₄, 809 cm⁻¹; CH₂Cl₂, 804 cm⁻¹; DMSO, 801 cm⁻¹) and attribute the band to the bending of the NO₂ group strongly coupled with the breathing motion of the adjacent thienyl ring. The frequency downshift is due to the softening with solvent polarity of the bonds mainly involved in the vibration. The N—O bonds lengthen by 0.005 Å, the C2′= C3′ and C4′=C5′ bonds by 0.005 Å, and the S′—C′ bonds by 0.003 Å.

Single-molecule DFT//B3LYP/6-31G** calculations usually provide vibrational spectra that nicely agree, after a proper scaling-down process of the frequencies, with the solid-state Raman features of many types of π-conjugated molecular materials.[18,21] This is not, however, the case for Me₂-T₂-NO₂, for which the theoretical "gas-phase" Raman spectrum shown on the top of Figure 6 is found to be rather different from that recorded for the pure solid sample (Figure 4, bottom). It follows that the solid-state packing forces and/or the extra polarization induced in the molecules of this push—pull system when they come close together in a well-ordered arrangement strongly affect the vibrational potential and the conjugational properties. This is in fact supported by the experimental spectra. As shown in Figure 4, the strongest Raman bands in the solid-state spectrum appear at lower frequencies than those recorded in the more polar DMSO solvent.

IV. Conclusions

The π-conjugated push—pull 5-(dimethylamino)-5′-nitro-2,2′-bithiophene chromophore has been investigated in a variety of solvents by using FT-Raman spectroscopy and DFT//B3LYP/6-31G** calculations. Theoretical calculations show that the molecule is highly polarized in the ground state because of the effective intramolecular charge transfer that takes place between the electron-donor and electron-acceptor end groups. The charge transfer is enhanced in passing to the first excited electronic state, and the molecule behaves as a very efficient photoinduced push—pull system.

Solvent effects have been taken into account by means of the Tomasi PCM model. As the polarity of the solvent increases, the intramolecular charge transfer is more effective, and the structure of the molecule becomes more quinoidized. In addition, more polar solvents produce a higher stabilization of the excited electronic state involved in the main optical absorption band, thus explaining the strong bathochromic shift the band undergoes with solvent polarity.

The large influence of the solvent on the molecular structure is strongly evidenced by the Raman spectra. The spectral profile greatly changes from one solvent to another and in passing to the solid. The Raman bands experimentally recorded have been found to undergo noticeable downshifts and intensity changes with increasing solvent polarity. The evolution of the Raman spectral profile with the solvent has been well-accounted for by the SCRF-PCM B3LYP/6-31G** calculations, which have provided a comprehensive assignment of the spectral features. In contrast to the nonpolar oligothiophenes, whose Raman spectra are dominated by the vibrations of the conjugated backbone, the strongest features in the spectrum of Me₂N-T₂-NO₂ correspond to the end-capping polar groups, even in a nonpolar solvent like CCl₄. The Raman spectrum recorded for the pure solid markedly differs from that calculated for a single molecule in a vacuum, which suggests that the intermolecular forces and/or the solid-state polarization exert a strong influence on the vibrational potential of this 5-(dimethylamino)-5′-nitro-2,2′-bithiophene.

References and Notes

(1) (a) Prasad, P. N.; Wiliams, D. J. *Introduction to Nonlinear Optical Effects in Molecvles and Polymers*; Wiley: New York, 1991. (b) Zyss, J. *Molecular Nonlinear Optics: Materials, Physics and Devices*; Academic Press: Boston, 1993. (c) Kanis, D. R.; Ratner, M. A.; Marks, T. J. *Chem. Rev.* **1994**, *94*, 195. (d) Marder, S. R.; Perry, J. W. *Adv. Mater.* **1993**, *5*, 804. (e) Marks, T. J.; Ratner, M. A. *Angew. Chem., Int. Ed. Engl.* **1995**, *34*, 155. (f) Dalton, L. R.; Harper, A. W.; Ghosn, R.; Steier, W. H.; Ziari, M.; Fetterman, H.; Shi, Y.; Mustacich, R. V.; Jen, A. K.-Y.; Shea, K. J. *Chem. Mater.* **1995**, *7*, 1060. (g) Shi, Y.; Zhang, C.; Bechtel, J. H.; Dalton, L. R.; Robinson, B. H.; Steier, W. H. *Science* **2000**, *288*, 119.

(2) (a) Verbiest, T.; Houbrechts, S.; Kauranen, M.; Clays, K.; Persoons, A. *J. Mater. Chem.* **1997**, *7*, 2175. (b) Wolf, J. J.; Wortmann, R. *Adv. Phys. Org. Chem.* **1999**, *32*, 121.

(3) (a) Long, N. J. *Angew. Chem., Int. Ed. Engl.* **1995**, *34*, 21. (b) Le Bozec, H.; Renouard, T. *Eur. J. Inorg. Chem.* **2000**, 229.

(4) (a) Marder, S. R.; Gorman, C. B.; Tiemann, B. G.; Cheng, L. T. *J. Am. Chem. Soc.* **1993**, *115*, 3006. (b) Marder, S. R.; Cheng, L. T.; Tiemann, B. G. *J. Chem. Soc., Chem. Commun.* **1992**, 672. (c) Cheng, L. T.; Tam. W.; Marder, S. R.; Steigman, A. E.; Rikken, G.; Spangler, C. W. *J. Phys. Chem.* **1993**, *95*, 10631 and 10643.

(5) (a) Marder, S. R.; Cheng, L. T.; Tiemann, B. G.; Friedli, A. C.; Blanchard-Desce, M.; Perry, J. W.; Skindhoj, J. *Science*, **1994**, *263*, 511. (b) Blanchard-Desce, M.; Alain, V.; Bedworth, P. V.; Marder, S. R.; Fort, A.; Runser, C.; Barzoukas, M.; Lebus, M. S.; Wortmann, R. *Chem.—Eur. J.* **1997**, *3*, 1091.

(6) Mignani, G.; Leising, F.; Meyreux, R.; Samson, H. *Tetrahedron Lett.* **1990**, *31*, 4743. (b) Jen, A. K.-Y.; Rao, V. P.; Drost, K. J.; Wong, K. Y.; Cava, M. P. *J. Chem. Soc., Chem. Commun.* **1994**, 2057. (c) Rao, V. P.; Cai, Y. M.; Jen, A. K.-Y. *J. Chem. Soc., Chem. Commun.* **1994**, 1689. (d) Jen, A. K.-Y.; Cai, Y. M.; Bedworth, P. V.; Marder, S. R. *Adv. Mater.* **1997**, *9*, 12.

(7) (a) Rao, V. P.; Jen, A. K.-Y.; Wong, K. Y.; Drost, K. J. *J. Chem. Soc., Chem. Commun.* **1993**, 1118. (b) Gilmour, S.; Montgomery, R. A.; Marder, S. R.; Cheng, L.-T.; Jen, A. K.-Y.; Cai, Y.; Perry, J. W.; Dalton, L. R. *Chem. Mater.* **1994**, *6*, 1603. (c) Boldt, P.; Bourhill, G.; Bräuchle, C.; Jim, Y.; Kammler, R.; Müller, C.; Rase, J.; Wichern, J. *J. Chem. Soc., Chem. Commun.* **1996**, 793. (d) Wu, X.; Wu, J.; Liu, Y.; Jen, A. K.-Y. *J. Am. Chem. Soc.* **1999**, *121*, 472. (e) Wu, X.; Wu, J.; Liu, Y.; Jen, A. K.-Y. *Chem. Commun.* **1999**, 2391.

(8) Sun, S.-S.; Zhang, C.; Dalton, L. R.; Garner, S. M.; Chen, A.; Steier, W. H. *Chem. Mater.* **1996**, *8*, 2539.

(9) Jen, A. K.-Y.; Liu, Y.; Zheng, L. Liu, S.; Drost, K. J.; Zhang, Y.; Dalton, L. R. *Adv. Mater.* **1999**, *11*, 452.

(10) (a) Rao, V. P.; Jen, A. K.-Y.; Wong, K. Y.; Drost, K. J. *Tetrahedron Lett.* **1993**, *34*, 1747. (b) Rao, V. P.; Wong, K. Y.; Jen, A. K.-Y.; Drost, K. J. *Chem. Mater.* **1994**, *6*, 2210. (c) Gilmour, S.; Marder, S. R.; Perry, J. W.; Cheng, L. T. *Adv. Mater.* **1994**, *6*, 494. (d) Steybe, F.; Effenberger, F.; Gubler, U.; Bosshard, C.; Günter, P. *Tetrahedron* **1998**, *54*, 8469. (e) Kim, O.-K.; Fort, A.; Barzoukas, M.; Blanchard-Desce, M.; Lehn, J.-M. *J. Mater. Chem.* **1999**, *9*, 2227. (f) Cai, C.; Liakatas, I.; Wong, M.-S.; Bösch, M.; Bosshard, C.; Günter, P.; Concilio, S.; Tirelli, N.; Suter, U. W. *Org. Lett.* **1999**, *1*, 1847. (g) Hutchings, M. G.; Ferguson, I.; McGeein, D. J.; Morley, J. O.; Zyss, J.; Ledoux, I. *J. Chem. Soc., Perkin Trans. 2* **1995**, 171.

(11) (a) Marder, S. R.; Perry, J. W.; Bourhill, G.; Gorman, C. B.; Tiemann, B. G.; Mansour, K. *Science* **1993**, *261*, 186. (b) Marder, S. R.; Gorman, C. B.; Meyers, F.; Perry, J. W.; Bourhill, G.; Brédas, J.-L.; Pierce, B. M. *Science* **1994**, *265*, 632.

(12) (a) Rao, V. P.; Jen, A. K.-Y.; Cai, Y. *J. Chem. Soc., Chem. Commun.* **1996**, 1237. (b) Wong, K. Y.; Jen, A. K.-Y.; Rao, V. P.; Drost, K. J.; Minnini, R. M. *Proc. SPIE-Int. Soc. Opt. Eng.* **1992**, 74. (c) Jen, A. K.-Y.; Cai, Y.; Bedworth, P. V.; Marder, S. R. *Adv. Mater.* **1997**, *9*, 132.

Solvent Effects on Intramolecular Charge Transfer

J. Phys. Chem. A, Vol. 109, No. 39, 2005 **8731**

(d) Raimundo, J.-M.; Blanchard, P.; Ledoux-Rak, I.; Hierle, R.; Michaux, L.; Roncali, J. *Chem. Commun.* **2000**, 1597. (e) Raimundo, J.-M.; Blanchard, P.; Frère, P.; Mercier, N.; Ledoux-Rak, I.; Hierle, R.; Roncali, J. *Tetrahedron Lett.* **2001**, *42*, 1507. (f) Raimundo, J.-M.; Blanchard, P.; Gallego-Planas, N.; Mercier, N.; Ledoux-Rak, I.; Hierle, R.; Roncali, J. *J. Org. Chem.* **2002**, *67*, 205.

(13) (a) Effenberger, F.; Würthner, F. *Angew. Chem., Int. Ed. Engl.* **1993**, *32*, 719. (b) Effenberger, F.; Würthner, F.; Steybe, F. *J. Org. Chem.* **1995**, *60*, 2082.

(14) Hartmann, H.; Eckert, K.; Schröder, A. *Angew. Chem., Int. Ed.* **2000**, *39*, 556.

(15) Würthner, F.; Effenberger, F.; Wortmann, R.; Krämer, P. *Chem. Phys.* **1993**, *173*, 305.

(16) Sakamoto, A.; Furukawa, Y.; Tasumi, M. *J. Phys. Chem.* **1994**, *98*, 4635.

(17) Yokonuma, N.; Furukawa, Y.; Tasumi, M.; Kuroda, M.; Nakayama, J. *Chem. Phys. Lett.* **1996**, *255*, 431.

(18) (a) Casado, J.; Hernández, V.; Hotta, S.; López Navarrete, J. T. *J. Chem. Phys.* **1998**, *109*, 10419. (b) Hernández, V.; Muguruma, H.; Hotta, S.; Casado, J.; López Navarrete, J. T. *J. Phys. Chem. A* **2000**, *104*, 735. (c) Hernández, V.; Calvo Losada, S.; Casado, J.; Higuchi, H.; López Navarrete, J. T. *J. Phys. Chem. A* **2000**, *104*, 661. (d) Moreno Castro, C.; Ruiz Delgado, M. C.; Hernández, V.; Hotta, S.; Casado, J.; López Navarrete, J. T. *J. Chem. Phys.* **2002**, *116*, 10419. (e) Moreno Castro, C.; Ruiz Delgado, M. C.; Hernández, V.; Shirota, Y.; Casado, J.; López Navarrete, J. T. *J. Phys. Chem. B* **2002**, *106*, 7163. (f) Casado, J.; Hicks, R. G.; Hernández, V.; Myles, D. J. T.; Ruiz Delgado, M. C.; López Navarrete, J. T. *J. Chem. Phys.* **2003**, *118*, 1912.

(19) (a) Casado, J.; Otero, T. F.; Hotta, S.; Hernández, V.; Ramírez, F. J.; López Navarrete, J. T. *Opt. Mater.* **1998**, *9*, 82. (b) Casado, J.; Hernández, V.; Hotta, S.; López Navarrete, J. T. *Adv. Mater.* **1998**, *10*, 1258. (c) Casado, J.; Maraver Puig, J. J.; Hernández, V.; Zotti, G.; López Navarrete, J. T. *J. Phys. Chem. A* **2000**, *104*, 10656. (d) Casado, J.; Katz, H. E.; Hernández, V.; López Navarrete, J. T. *J. Phys. Chem. B* **2002**, *106*, 2488. (e) Casado, J.; Miller, L. L.; Mann, K. R.; Pappenfus, T. M.; Hernández, V.; López Navarrete, J. T. *J. Phys. Chem. B* **2002**, *106*, 3597. (f) Casado, J.; Miller, L. L.; Mann, K. R.; Pappenfus, T. M.; Kanemitsu, Y.; Ortí, E.; Viruela, P. M.; Pou-Amérigo, R.; Hernández, V.; López Navarrete, J. T. *J. Phys. Chem. B* **2002**, *106*, 3872. (g) Casado, J.; Ruiz Delgado, M. C.; Shirota, Y.; Hernández, V.; López Navarrete, J. T. *J. Phys. Chem. B* **2003**, *107*, 2637. (h) Casado, J.; Miller, L. L.; Mann, K. R.; Pappenfus, T. M.; Higuchi, H.; Ortí, E.; Milián, B.; Pou-Amérigo, R.; Hernández, V.; López Navarrete, J. T. *J. Am. Chem. Soc.* **2002**, *124*, 12380. (i) Casado, J.; Pappenfus, T. M.; Miller, L. L.; Mann, K. R.; Ortí, E.; Viruela, P. M.; Pou-Amérigo, R.; Hernández, V.; López Navarrete, J. T. *J. Am. Chem. Soc.* **2003**, *125*, 2524.

(20) Hernández, V.; Casado, J.; Effenberger, F.; López Navarrete, J. T. *J. Chem. Phys.* **2000**, *112*, 5105.

(21) (a) González, M.; Segura, J. L.; Seoane, C.; Martín, N.; Garín, J.; Orduna, J.; Alcala, R.; Villacampa, B.; Hernández, V.; López Navarrete, J. T. *J. Org. Chem.* **2001**, *66*, 8872. (b) Ruiz Delgado, M. C.; Hernández, V.; Casado, J.; López Navarrete, J.-M.; Blanchard, P.; Roncali, J. *Chem.—Eur. J.* **2003**, *9*, 3670. (c) Milián, B.; Ortí, E.; Hernández, V.; López Navarrete, J. T.; Otsubo, T. *J. Phys, Chem. B* **2003**, *107*, 12175. (d) Casado, J.; Hernández, V.; Kim, O.-K.; Lehn, J.-M.; López Navarrete, J. T.; Delgado Ledesma, S.; Ponce Ortiz, R.; Ruiz Delgado, M. C.; Vida, V.; Pérez-Inestrosa, E. *Chem.—Eur. J.* **2004**, *10*, 3805.

(22) (a) Zerbi, G.; Castiglioni, C.; Del Zoppo, M. *Electronic Materials: The Oligomer Approach*; Wiley-VCH: Weinheim, 1998; p 345. (b) Castiglioni, C.; Gussoni, M.; López Navarrete, J. T.; Zerbi, G. *Solid State Commun.* **1988**, *65*, 625. (c) López Navarrete, J. T.; Zerbi, G. *J. Chem. Phys.* **1991**, *94*, 957 and 965. (d) Hernández, V.; Castiglioni, C.; Del Zoppo, M.; Zerbi, G. *Phys. Rev. B* **1994**, *50*, 9815. (e) Agosti, E.; Rivola, M.; Hernández, V.; Del Zoppo, M.; Zerbi, G. *Synth. Met.* **1999**, *100*, 101.

(23) (a) Ehrendorfer, Ch.; Karpfen, A. *J. Phys. Chem.* **1994**, *98*, 7492. (b) Ehrendorfer, Ch.; Karpfen, A. *J. Phys. Chem.* **1995**, *99*, 5341.

(24) (a) Miertus, S.; Scrocco, E.; Tomasi, J. *Chem. Phys.* **1981**, *55*, 117. (b) Miertus, S.; Tomasi, J. *Chem. Phys.* **1982**, *65*, 239. (c) Cossi, M.; Barone, V.; Cammi, R.; Tomasi, J. *Chem. Phys. Lett.* **1996**, *255*, 327. (d) Cances, M. T.; Mennucci, B.; Tomasi, J. *J. Chem. Phys.* **1997**, *107*, 3032. (e) Barone, V.; Cossi, M.; Tomasi, J. *J. Comput Chem.* **1998**, *19*, 404. (f) Cossi, M.; Scalmani, G.; Rega, N.; Barone, V. *J. Chem. Phys.* **2002**, *117*, 43.

(25) Frisch, M. J.; Trucks, G. W.; Schlegel, H. B.; Scuseria, G. E.; Robb, M. A.; Cheeseman, J. R.; Montgomery, J. A.; Vreven, T. Jr.; Kudin, K. N.; Burant, J. C.; Millam, J. M.; Iyengar S. S.; Tomasi, J.; Barone, V.; Mennucci, B.; Cossi, M.; Scalmani, G.; Rega, N.; Petersson, G. A.; Nakatsuji, H.; Hada, M., Ehara, M.; Toyota, K.; Fukuda, R.; Hasegawa, J.; Ishida, M.; Nakajima, T.; Honda, Y.; Kitao, O.; Nakai, H.; Klene, M.; Li, X.; Knox, J. E.; Hratchian, H. P.; Cross, J. B.; Adamo, C.; Jaramillo, J.; Gomperts, R.; Startmann, R. E.; Yazyev, O.; Austin, A. J.; Cammi, R.; Pomelli, C.; Ochterski, J. W.; Ayala, P. Y.; Morokuma, K.; Voth, G. A.; Salvador, P.; Dannenberg, J. J.; Zakrzewski, V. G.; Dapprich, J. M.; Daniels, A. D.; Strain, M. C.; Farkas, O.; Malick, D. K.; Rabuck, A. D.; Raghavachari, K.; Foresman, J. B.; Ortiz, J. V.; Cui, Q.; Baboul, A. G.; Cliffors, S.; Cioslowski, J.; Stefanov B. B.; Liu, G.; Liashenko, A.; Piskorz, I.; Komaromi, I.; Martin R. L.; Fox, D. J.; Keith, T.; Al-Laham, M. A.; Peng, C. Y.; Manayakkara, A.; Challacombe, M.; Gill, P. M. W.; Johnson, B. G.; Chen, W.; Wong, M. W.; Gonzalez, C.; Pople, J. A. *Gaussian 2003,* revision C.02; Gaussian, Inc.: Pittsburgh, PA, 2003.

(26) Becke, A. D. *J. Chem. Phys.* **1993**, *98*, 1372.

(27) Francl, M. M.; Pietro, W. J.; Hehre, W. J.; Binkley, J. S.; Gordon, M. S.; Defrees, D. J.; Pople, J. A. *J. Chem. Phys.* **1982**, *77*, 3654.

(28) Scott, A. P.; Radom, L. *J. Phys. Chem.* **1996**, *100*, 16502.

(29) Rauhut, G.; Pulay, P. *J. Phys. Chem.* **1995**, *99*, 3093. Carbonniere, P.; Lucca, T.; Pouchan, C.; Rega, N.; Barone, V. *J. Comput. Chem.* **2005**, *26*, 384.

(30) (a) Runge, E.; Gross, E. K. U. *Phys. Rev. Lett.* **1984**, *52*, 997. (b) Gross, E. K. U.; Kohn, W. *Adv. Quantum Chem.* **1990**, *21*, 255. (c) Gross, E. K. U.; Ullrich, C. A.; Gosssman, U. J. In *Density Functional Theory*; Gross, E. K. U., Driezler, R. M., Eds.; Plenum Press: New York, 1995; p 149.

(31) Casida, M. E. in *Recent Advances in Density Functional Methods, Part I*; Chong, D. P., Ed.; World Scientific: Singapore, 1995; p 155.

(32) Koch, W.; Holthausen, M. C. *A Chemist's Guide to Density Functional Theory*; Wiley-VCH: Weinheim, Germany, 2000.

(33) Tomasi, J.; Persico, M. *Chem. Rev.* **1994**, *94*, 2027. (b) Cramer, C. S.; Truhlar, D. G. In *Solvent Effects and Chemical Reactivity*; Tapia, O., Bertrán, J., Eds.; Kluwer: Dordrecht, 1996; p 1.

(34) Cappelli, C.; Corni, S.; Cammi, R.; Mennucci, B.; Tomasi, J. *J. Chem. Phys.* **2000**, *113*, 11270.

(35) Cappelli, C.; Corni, S.; Tomasi, J. *J. Chem. Phys.* **2001**, *115*, 5531.

(36) (a) Reed, A. E.; Weinhold, F. *J. Chem. Phys.* **1983**, *78*, 4066. (b) Reed, A. E.; Weinstock, R. B.; Weinhold, F. *J. Chem. Phys.* **1985**, *83*, 735.

(37) Reed, A. E.; Curtiss, L. A.; Weinhold, F. *Chem. Rev.* **1988**, *88*, 899.

(38) NPA charges were calculated for Me_2-T_2-NO_2 using the more extended correlation-consistent aug-cc-pVDZ basis set (Kendall, R. A.; Dunning, T. H., Jr.; Harrison, R. J. *J. Chem. Phys.* **1992**, *62*, 6796). The charges calculated differ by less than 0.02 e from those quoted in the text. The inclusion of diffuse functions in the basis set has almost no effect on the description obtained for the intramolecular charge transfer.

(39) The use of the aug-cc-pVDZ basis set slightly reduces the excitation energies but leads to identical trends (n-hexane, 2.42 eV; CCl$_4$, 2.39 eV; CH$_2$Cl$_2$, 2.30 eV; DMSO, 2.25 eV).

(40) Hernández, V.; Casado, J.; Ramírez, V. J.; Zotti, G.; Hotta, S.; López Navarrete, J. T. *J. Chem. Phys.* **1996**, *104*, 9271.